Talanta 253 (2023) 124008

Contents lists available at ScienceDirect

Talanta

journal homepage: www.elsevier.com/locate/talanta

A SARS-CoV-2 impedimetric biosensor based on the immobilization of ACE-2 receptor-containing entire cell membranes as the biorecognition element

Juliana Cancino-Bernardi [a,b,*], Edson José Comparetti [a], Natalia Noronha Ferreira [a], Renata Rank Miranda [a], Marco Montero Tuesta [a], Isabella Sampaio [a], Paulo Inácio da Costa [c], Valtencir Zucolotto [a,**]

[a] Nanomedicine and Nanotoxicology Group, Physics Institute of São Carlos, University of São Paulo, São Carlos, SP, Brazil
[b] Bioanalytics of Nanosystems Laboratory, Department of Chemistry, FFCLRP-USP, University of São Paulo – USP, Ribeirão Preto, SP, Brazil
[c] School of Pharmaceutical Sciences, São Paulo State University, Department of Clinical Analysis, Laboratory of Clinical Immunology and Molecular Biology, Araraquara, São Paulo, Brazil

ARTICLE INFO

Keywords:
SARS-CoV-2
Covid-19
Biosensor
ACE-2 transmembrane receptor

ABSTRACT

A SARS-CoV-2 biosensor based on the biorecognition of the spike protein to the angiotensin-converting enzyme 2 (ACE-2) transmembrane receptor was developed using entire cell membranes as the biorecognition layer. In this new SARS-CoV-2 detection platform, cellular membranes from VeroCCL81 (mVero) and Calu-3 (mCalu) cells (which overexpress the ACE-2 transmembrane receptors) were extracted and immobilized as vesicles on an indium tin oxide electrode (ITO). Electrochemical impedance spectroscopy was used to optimize the performance of the developed devices for SARS-CoV-2 detection. This novel biosensor comprises a low-cost system (less than one US$ dollar) that uses the unique properties of cell membranes combined with the catalytic properties of electrochemical platforms to allow spike proteins recognition. A linear response from 10 to 100 ng/mL was obtained from the optimized biosensors, a limit of detection of 10.0 pg/mL and 7.25 pg/mL and limit of quantification of 30.4 pg/mL and 21.9 pg/mL were achieved with satisfactory accuracy for ITO-APTES-mVero and ITO-APTES-mCalu, respectively. Selectivity studies revealed that this platform was able to differentiate the target spike proteins from NS1 proteins from dengue and Zika viruses. In addition, sensors comprising cell membranes devoid of the ACE-2 transmembrane receptor exhibited no biorecognition signal. The developed devices are suitable for SARS-CoV-2 detection based on spike protein recognition, and capable of providing a low-cost, accurate, and accessible tool for use in a pandemic and post-pandemic scenario.

1. Introduction

Diagnostic systems have been shown to be key elements required for the control of positive cases during the SARS-CoV-2 pandemic, making it possible to create isolation strategies. Currently, the gold-standard diagnostic test commonly used to detect SARS-CoV-2 infections is the reverse transcriptase-polymerase chain reaction (RT-PCR) [1]. This system exhibits very high sensitivity and efficiency; however, it is expensive, requires specialized non-portable equipment, and rely on operator expertise for their interpretation, being unavailable to the majority of the population. As an alternative, rapid tests to detect SARS-CoV-2 antibodies or infectious viral antigens are purely qualitative in nature (i.e., they only indicate the presence or absence of SARS-CoV-2 antibodies) have been widely developed and marketed [2–4]. However, the inefficient detection window in relation to the viral cycle, as well as the large number of false-positive and false-negative results have been considered the main limitations for these rapid tests [5].

* Corresponding author. Chemistry Department, Faculty of Philosophy, Sciences and Letters of Ribeirão Preto - FFCLRP University of São Paulo - USP, Av. Bandeirantes 3900, CEP 14040-901, Ribeirão Preto, São Paulo State, Brazil.
** Corresponding author. Nanomedicine and Nanotoxicology Group, Physics Institute of São Carlos, University of São Paulo, Av. Trabalhador Sãocarlense 400, CEP 13566-590, São Carlos, São Paulo State, Brazil.
E-mail addresses: jucancino@usp.br (J. Cancino-Bernardi), zuco@ifsc.usp.br (V. Zucolotto).

https://doi.org/10.1016/j.talanta.2022.124008
Received 6 July 2022; Received in revised form 6 October 2022; Accepted 11 October 2022
Available online 22 October 2022

To improve the specificity and selectivity of SARS-CoV-2 biosensors, one receptor has attracted attention in relation to its high specificity in the recognition of the virus via the SARS-CoV-2 spike protein: the angiotensin-converting enzyme 2 (ACE-2) transmembrane receptor. It is well known that SARS-CoV-2 infects mammalian cells through a receptor recognition mechanism mediated by the transmembrane glycoprotein spike located on the surface of the viral envelope [6]. This glycoprotein has a receptor-binding domain that specifically binds to the ACE-2 receptor [7,8]. ACE-2 is expressed on the surface of several epithelial cells of the nasal mucosa, bronchi, and lungs, but also in other tissues such as the heart, kidney, and intestine [9–12]. The expression pattern of ACE-2 in different organs, tissues, and cell types may be directly associated with SARS-CoV-2 infection, since target cells that express high levels of ACE-2 may allow greater entry, multiplication, dissemination, and pathogenesis of this coronavirus [13].

Several *in vitro* study models, such as mammalian cell lines, have been successfully used in research related to SARS-CoV-2. An important feature of these models is their high susceptibility to the virus, which is directly related to the expression of ACE-2 and type II transmembrane serine proteases (TMPRSS2). Among human cell lines, Calu-3, Caco-2, and Huh7 have high levels of expression of these proteins [14]. In contrast, A549 cells express low levels of ACE-2 and are not easily infected by SARS-CoV-2 [14]. In addition, VeroCCL81 cells, isolated from the renal epithelial cells of an African green monkey, are widely used in research related to SARS-CoV-2 because they are easily infected by the virus due to the presence of high levels of ACE-2 on their surface [14,15].

The use of biorecognition between cell membranes that express the ACE-2 receptors and the virus spike protein may be a new and efficient way to diagnose SARS-CoV-2, especially in terms of the cost of production and isolation, when compared to other targets. Combined with a highly selective biorecognition layer, electrochemical biosensors can offer greater access to the identification of the spike virus related to SARS-CoV-2. Such biosensors are of very high interest, mainly because of their versatility, simplicity, high miniaturization potential, and low cost. Torres et al. and Lima et al. recently developed point-of-care biosensors for SARS-CoV-2 diagnosis based on ACE-2 antibodies [16,17]. The biosensor, called RAPIS 1.0, exhibited a sensitivity and specificity of c. a. 85%–100% for nasopharyngeal and oropharyngeal specimen samples [16]. The detection of the second biosensor, LEAD, was measured via square wave voltammetry, reaching a detection limit of 229 fg/mL for the spike protein [17]. In both cases, the authors used commercially supplied ACE-2 enzyme immobilized on the surface of graphite electrodes coated with gold nanoparticles. The system differs from the one presented here, which uses entire membranes of specific cells as a biorecognition layer, improving specificity and significantly decreasing the cost of the sensor.

The main objective of this study was to develop a biosensor using a biorecognition layer comprising entire cell membranes abundant in ACE-2 transmembrane receptors. For this, cell membranes with high expression of the ACE-2 receptor were extracted from VeroCCL81 and Calu-3 cells and conjugated with *N*-ethyl-*N*'-(3-dimethylaminopropyl) carbodiimide hydrochloride (EDC) and *N*-hydroxysuccinimide (NHS) for the construction of membrane vesicles obtained by mechanical extrusion. The VeroCCL81 and Calu-3 cell lines were chosen because they overexpress the ACE-2 transmembrane receptor, which has aroused much interest as a key element in the development of vaccines against COVID-19. The membrane/EDC/NHS vesicles were then immobilized on an indium tin oxide (ITO) electrode modified with an amino-silane group. Electrochemical impedance spectroscopy (EIS) analyses showed that the system was able to recognize the SARS-CoV-2 spike protein with high specificity, exceeding its selectivity for the NS1 proteins of dengue and Zika viruses, used as interferents.

2. Material and methods

2.1. Materials and reagents

(3-Aminopropyl) triethoxysilane (APTES) and potassium hexacyanoferrate (II) trihydrate were obtained from Sigma-Aldrich, Brazil. Propanone, isopropyl alcohol, and ethanol were obtained from Synth (Brazil). Measurement solutions containing potassium hexacyanoferrate (II) trihydrate were prepared in a phosphate buffer (PB 0.1 mol/L, pH 7.4) and maintained at 18 °C. Ultrapure water (resistance >18 MΩ/cm) used in all experiments was obtained using a Mega Purity purification system. All glassware was kept in 10% (v/v) HNO_3 solution for cleaning and washed thoroughly with ultrapure water before use.

For detection measurements, three electrodes were used: a 1.3 cm^2 platinum plate counter electrode, Ag/AgCl in KCl (3.0 mol/L) as the reference electrode and ITO (originally obtained from Delta Technologies) with a resistance of 8–12 Ω and geometric area of 0.5 cm^2 as the working electrode. All electrochemical measurements were performed with an Autolab® potentiostat equipped with GPES 4.9 and FRA 4.9 software. Cyclic voltammetry (CV) was performed at a scanning rate of 100 mV s^{-1} and the potential varied between −200 and 800 mV. For EIS measurements, a sinusoidal signal with an amplitude of 10 mV was applied over the open cell potential in the frequency range of 0.1–10,000 Hz. The charge transfer resistances (R_{ct}) were evaluated with respect to the geometric area of the ITO, and thus, the obtained results were analyzed using ΔR_{ct}.

2.2. Isolation of the cell membrane containing ACE-2 receptors

Cell membranes were isolated and purified according to the method proposed by Lund et al. [18]. VeroCCL81 (healthy African green monkey kidney epithelial) and Calu-3 (human lung adenocarcinoma epithelial) cells were grown as a monolayer in DMEM medium (Dulbecco's modified Eagle's medium, Vitrocell, Campinas, Brazil) supplemented with 10% fetal bovine serum (Vitrocell, Campinas, Brazil), in 150 cm^2 flasks, until they reached approximately 90% confluence. The flasks were rinsed with PBS at 4 °C, then 5 mL of ice-cold phosphate buffer saline (PBS 0.1 mol/L, pH 7.4) was added, and the cells were removed with the aid of a cell spreader. The collected cells were washed three times by centrifugation (1000 g, 5 min) with PBS at 4 °C and lysed in a hypotonic buffer (10 mmol/L Tris base, 1.5 mmol/L $MgCl_2$, 10 mmol/L NaCl, pH 6.8) for 20 min on ice. After this period, the lysed cells were centrifuged (300 g, 5 min), resuspended in gradient buffer (0.25 mol/L sucrose, 10 mmol/L HEPES, 100 mmol/L succinic acid, 1 mmol/L EDTA, 2 mmol/L $CaCl_2$, 2 mmol/L $MgCl_2$, pH 7.4), homogenized through 80 cycles (1900 rev/min) in a homogenizer (Glass homogenizer VIRTUS PII) and centrifuged at 10,000 g for 10 min. The supernatant was collected and centrifuged at 100,000 g for 2 h in an Optima MAX-XP ultracentrifuge (Beckman Coulter, USA). The pellet containing the cell membrane vesicles was resuspended in PBS containing protease inhibitors (Roche Diagnostics, Mannheim, Germany) and stored in a freezer at −80 °C. The yield of each extracted membrane was measured by Nanotracking analysis (NTA), resulting in 2×10^{11} particles/mL for mCalu and 1.5×10^{11} particles/mL for mVero.

2.3. Characterization of ACE-2 receptor vesicles

Subsequently, the extracted cell membranes were kept in a dry bath with EDC/NHS (8 mmol/L and 5 mmol/L, respectively) at 37 °C for 8 h in PB. The system was then extruded through the membrane using a mini-extruder (Avanti Polar Lipids) with 100 nm pores. The resulting system was then characterized as a function of size, charge, and concentration using dynamic light scattering (DLS), zeta potential, and nano tracking analyzer (NTA) techniques, respectively.

2.4. Fabrication of the membrane biosensors

The membrane biosensors were fabricated in three steps, as illustrated in Fig. 1.

Initially, the 1 × 0.5 cm^2 ITO electrodes underwent chemical cleaning via immersion in acetone and sonication for 10 min. The process was repeated using isopropyl alcohol, ethanol, and ultrapure water. Subsequently, the electrodes were dried under N_2 flow and modified with the immobilization of APTES. The electrodes were immersed for 1 h in a solution containing 2% v/v of APTES in ethanol. After incubation, the electrode was carefully washed with ultrapure water and dried using inert N_2 gas. Finally, the device was immersed in a dispersion of cell membrane vesicles/EDC/NHS (concentrations of 10^6, 10^7, or 10^8 particles/mL) containing the ACE-2 receptor for 1 h 30 min (PB 0.1 mol/L, pH 7.4). The incubation time was varied between 1 and 2 h. It is important to note that this dispersion must be kept in ice and be prepared 48 h before immobilization on the ITO electrode. After each step, the electrodes were carefully washed with ultrapure water and dried under a stream of N_2.

2.5. Detection of the SARS-CoV-2 spike protein

The performance of membrane biosensors was evaluated after each step of their construction. For this, $K_4Fe(CN)_6$ (4 mmol/L) redox group was used to monitor indirectly the impedimetric binding of the spike protein to mVero or mCalu at the electrode surface. Since it refers to a biorecognition binding of the molecules, the electrochemical measurements were based on changes in the electron transfer resistance of the redox couple which is directly related to the protein-ACE2 membrane interaction. The detection process occurred in two steps: First, membrane biosensors were immersed in 1 mL of PB buffer solution containing spike protein at different concentrations (depending on the evaluated parameter) for an optimized incubation time of 30 min at room temperature. Then, the membrane biosensors were removed from the solution and rinsed by immersion in 2 mL of PB buffer to remove the excess of non-adsorbed molecules. Afterwards, the protein-ACE2 membrane biorecognition process was monitored indirectly by CV and EIS using $K_4Fe(CN)_6$ (4 mmol/L) redox groups. All measurements were performed in triplicate in at least three independent experiments, and at an average temperature of 17–19 °C.

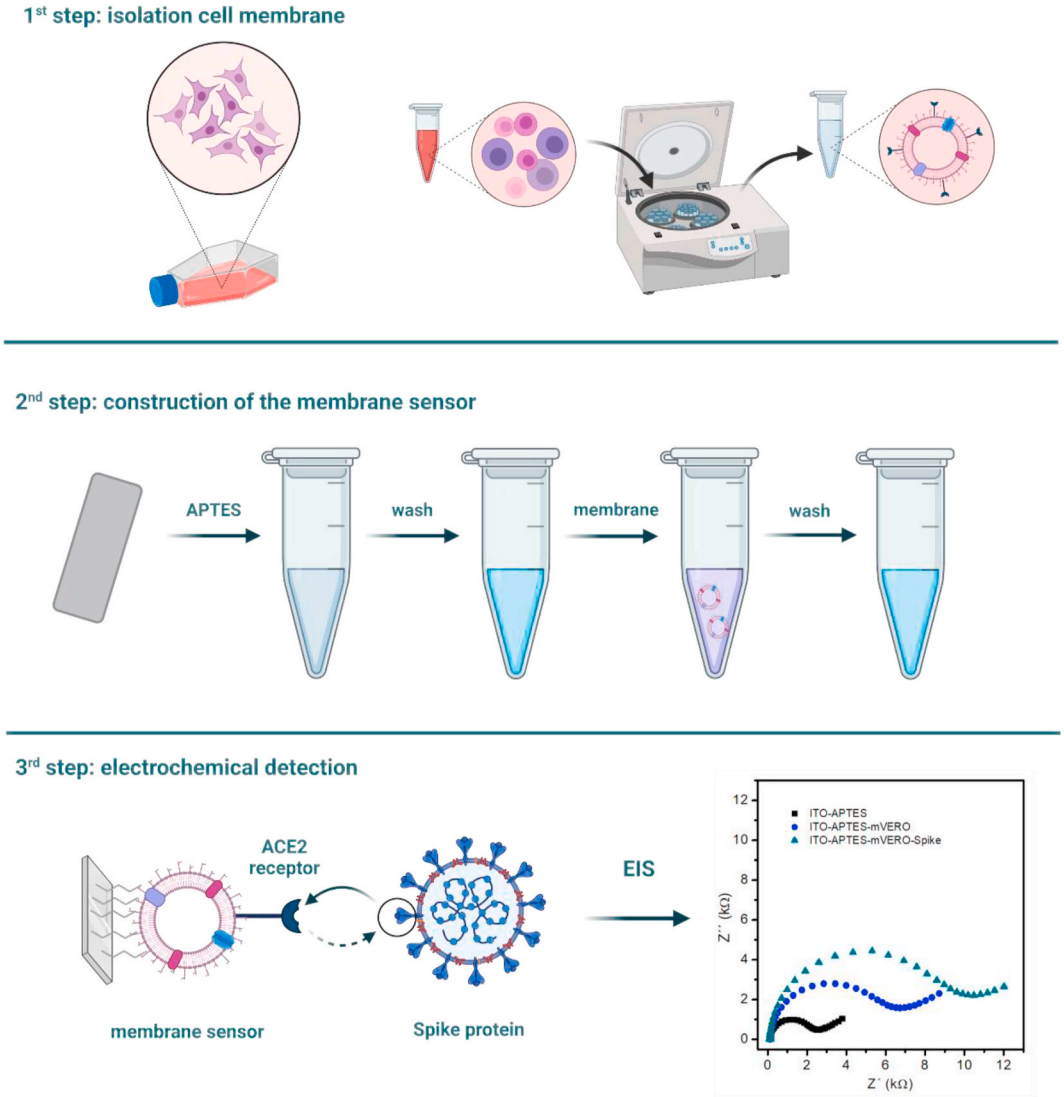

Fig. 1. Schematic representation of the construction of the membrane sensors comprising ITO-APTES-mCalu and ITO-APTES-mVero membranes. The first step was based on the isolation of Vero and Calu cells membranes by ultracentrifugation, followed by mechanical extraction in 100 nm membrane pores. The second step represents the adsorption of APTES and membrane vesicles containing EDC/NHS on ITO electrode surfaces by covalent bind using the self-assembly technique. The last step is the electrochemical impedance spectroscopy measurement to detect the SARS-CoV-2 spike protein via ACE-2 receptor biorecognition localized at the biorecognition cell membrane element. Figure created with BioRender.com.

The working concentration range for the spike protein ranged from 10 to 120 ng/mL. The linearity of the system was evaluated by applying a linear regression at a 95% confidence level, as well as by the regression coefficient (R^2). The limits of detection (LOD) and quantification (LOQ) of each antigen were calculated according to equations (1) and (2) [19,20]:

$$LOD = \frac{3.3 * S_b}{m} \quad (1)$$

$$LOQ = \frac{10 * S_b}{m} \quad (2)$$

where S_b represents the standard deviation of 10 blank samples (the response of the biosensor without the spike protein) and m corresponds to the slope of the corresponding analytical curve.

2.6. Selectivity of the membrane biorecognition layer

The specificity of the membrane biosensors was analyzed by incubating the biosensors in a solution containing 25 ng/mL of NS1 proteins from dengue and Zika viruses for 50 min and compared with the SARS-CoV-2 spike protein (positive target) response in terms of ΔR_{ct}. The specificity of the biorecognition layer was checked using membranes with a low expression of the ACE-2 receptor (A549 lung carcinoma, ATCC number CCL-185) as well as a synthetic liposome (composition based on the lipid dipalmitoylphosphatidylcholine - DPPC) without any receptors, immobilized on the surface of the ITO electrode through the same procedure reported in 2.4. These biosensors were evaluated as a function of their biorecognition using 50 ng/mL of the spike protein. Importantly, in the absence of the ACE-2 receptor, no EIS response was observed.

2.7. Characterization of the membrane biosensor surface

The ITO-APTES-mVero and ITO-APTES-mCalu surfaces were investigated by atomic force microscopy (AFM) and Raman spectroscopy before and after interaction with the SARS-CoV-2 spike protein. Images were collected using a FLEX-AFM atomic force microscope (Nanosurf, Switzerland) operated in intermittent contact mode. A silicon cantilever Tap300-G from Budget Sensors with a spring constant of 40 N/m was used. All experiments were performed at room temperature. Raman spectra were collected with an inVia™ Raman microscope (Renishaw, UK) using a 50 × Zeiss air objective. The samples were excited by a 532 nm laser using a power of 500 μW and an acquisition time of 10 s.

3. Results and discussion

3.1. Cell membrane vesicles and membrane biosensor characterization

Prior to immobilizing the cell membrane vesicles (biorecognition layer) on the electrode surface, the size and surface charge of the ACE-2 membrane vesicles were investigated by dynamic light scattering (DLS), nanoparticle tracking analysis (NTA) and zeta potential measurements, as shown in Table 1.

Table 1
Size and zeta potential values of Vero and Calu membranes vesicles based on NTA and DLS data.

VESICLES	SIZE (nm)		ZETA POTENTIAL (mV)
	NTA	DLS	
MNPs mVERO	143 ± 2	190 ± 4	−9.6 ± 0.5
MNPs mVERO[a]	162 ± 1	336 ± 7	−8.9 ± 0.5
MNPs mCALU	137 ± 2	279 ± 4	−9.2 ± 0.3
MNPs mCALU[a]	159 ± 5	319 ± 10	−11 ± 1

[a] Without EDC/NHS.

As shown in Table 1, the vesicles from mVero cells exhibited a mean size of 190 ± 4 nm and 142 ± 2 nm, as measured by DLS and NTA, respectively. The introduction of EDC/NHS molecules to the vesicles affects the size pattern, corresponding to an increase in the mVero vesicle sizes of ~140 nm and ~20 nm, as measured by DLS and NTA, respectively. The latter showed that EDC/NHS was efficiently incorporated through the mVero membrane to form vesicles. The same behavior was observed for mCalu vesicles, with mean sizes of 279 ± 4 nm and 137 ± 2 nm according to DLS and NTA measurements, respectively. An increase in the size of ~22 nm for NTA and 40 nm for DLS was also observed when EDC/NHS was incorporated through the mCalu membrane. The latter results revealed a lower variation in the zeta potential values — from −9.6 ± 0.5 to −8.4 ± 0.5 mV for mVero and from −9.2 ± 0.3 to −11 ± 1 mV for mCalu — due to EDC/NHS incorporation through the membranes. These changes were expected because of the different biomolecules present at the cell surface that contribute to the surface charge. Previous studies with membranes extracted from cells revealed similar behaviors in terms of size and surface charge [21–23].

Once the mCalu and mVero membrane vesicles were immobilized on the ITO electrodes modified with APTES, the surface morphology was characterized by AFM and Raman spectroscopy, as shown in Fig. 2A.

The AFM images show that mVero and mCalu adsorbed to the surface of ITO-APTES in a homogeneous manner, increasing the rugosity of the surface, as shown in support information Table SI1. Upon interaction with the SARS-CoV-2 spike proteins, a change in the biorecognition surface is observed, which present a higher rugosity and a soft pattern surface, especially for the ITO-APTES-mCalu electrodes, which had their rugosity increased from 2.18 nm to 8.43 nm, as revealed by AFM images. The Raman spectra of the membrane biosensors are shown in Fig. 2B and C. The peak at 1096 cm^{-1} [24] is characteristic of the ITO electrode. Functionalization of the ITO electrode with APTES did not produce significant changes in the Raman spectrum, which was probably due to its low concentration. However, after incubation with cell membranes, both sensors exhibited three peaks in the region of 2900 cm^{-1}, which arise from C–H_2 antisymmetric stretching of lipids, CH_3 symmetric stretching of proteins and lipids, and C–H stretching of lipids [25,26], demonstrating the efficient mVero e mCalu vesicles immobilization on the ITO electrodes.

3.2. Detection measurements

The detection of the SARS-CoV-2 spike proteins using the membrane as recognition layer is shown in Fig. 3, which depicts the cyclic voltammograms and Nyquist diagrams for the ITO-APTES-mVero and ITO-APTES-mCalu impedimetric biosensors. For both electrodes, an increase in the ΔR_{ct} values is observed after each surface change modification, whereas the current values related to each modification step decrease because of the impedimetric response of the redox probe signal. It is possible to observe that the peak current related to the silanization process is slightly higher, whereas the value of ΔR_{ct} is lower than that in the subsequent steps. After immobilization of the mVero or mCalu, there was an increase in ΔR_{ct} of 4.06 kΩ for the ITO-APTES-mVero and 3.35 kΩ for the ITO-APTES-mCalu sensors, because of the blockade of the APTES binding sites on the electrode surface.

Upon interaction with the SARS-CoV-2 spike proteins, a significant increase in ΔR_{ct} was observed. In this step, a further increase of ΔR_{ct} occurred, indicating the biorecognition of spike proteins and ACE-2 receptors, resulting in an increase in ΔR_{ct} of 4.33 kΩ for the ITO-APTES-mVero and 8.11 kΩ for the ITO-APTES-mCalu sensors. The ITO-APTES-mCalu biosensor had a higher ΔR_{ct} value, compared to the ITO-APTES-mVero system, because of the higher amount of ACE-2 transmembrane receptors on its surface, which improved the spike protein recognition, as revealed by flow cytometry analysis. The immobilization steps also affected probe oxidation, with a decrease in the current and a shift to higher potentials, indicating a decrease in electron transfer of the K_4 [$Fe(CN)_6$] redox molecules to the electrode

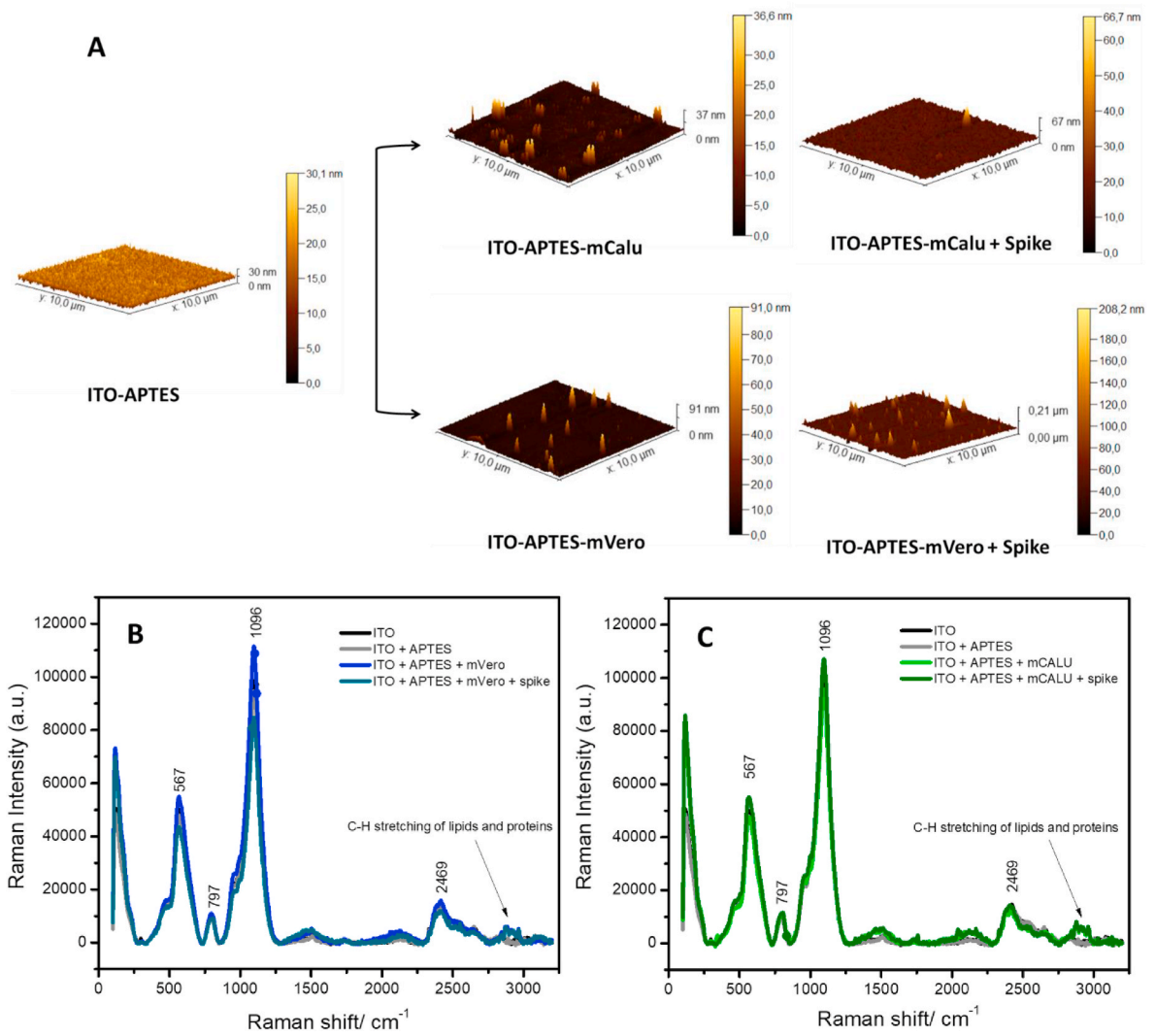

Fig. 2. (A) AFM images and Raman spectra of (B) Vero and (C) Calu membrane biosensors in different steps of their construction: ITO, ITO/APTES, ITO/APTES/mVero, ITO/APTES/mCalu, ITO/APTES/mVero/spike and ITO/APTES/mCalu/spike.

surface, due to the higher layer resistance. After mVero vesicles immobilization on the electrode surface, the system exhibited a decrease in the redox oxidation peak, which varied from 48 μA to 44 μA, as well as a shift from 389 to 487 mV. Upon spike biorecognition by the ACE-2 receptors, the redox oxidation peak varied from 44 μA to 32 μA, but the potential remains at 487 mV. Similar values were observed when mCalu vesicles were attached to the ITO-APTES electrode surface. The adsorption of mCalu vesicles to the ITO-APTES surface resulted in a decrease in the redox oxidation current from 49 μA to 30 μA, as well as a shift in the potential from 366 to 443 mV. Upon spike biorecognition by the ACE-2 receptors, the redox oxidation current varied from 30 to 24 μA, and the potential increased to 460 mV.

3.3. *Specificity and selectivity of the membrane biosensor*

To test the specificity of membrane biosensors toward SARS-CoV-2 spike proteins, detection measurements were performed with membrane vesicles extracted from cells with a low expression of the ACE-2 receptor (A549 cells) and with synthetic DPPC vesicles (ITO-APTES-mA549 and ITO-APTES-LP membrane sensors). As shown in support information Fig. SI-1A, the ITO-APTES-LP impedimetric biosensor was not able to detect SARS-CoV-2 spike proteins, compared to ITO-APTES-mVero or ITO-APTES-mCalu sensors. No significant ΔR_{ct} occurred after ITO-APTES-LP exposure to 25 ng/mL of spike protein for 40 min. Although ITO-APTES-mA549 (Fig. SI–1B) had an increase of 0.20 kΩ in the resistance of the electron transfer, it was at least 20 times lower than that observed with ITO-APTES-mVero, or 40 times lower than that with the ITO-APTES-mCalu sensors. This response may be associated with the lower amount of ACE-2 transmembrane receptor expressed at the cell surface, creating fewer active binding sites available for the spike protein recognition.

To compare the selectivity of the membrane biosensors developed here toward other viruses, NS1 biomarker proteins from dengue fever (NS1denV) and Zika (NS1zikV) were used. The results are shown as Nyquist plots in support information Fig. SI-1 C–F. Even with the weak detection of NS1denV and NS1zikV viruses from both membrane sensors, probably due to unspecific adsorption, it is noted that both constructed membrane impedimetric biosensors can differentiate them from the SARS-CoV-2 spike proteins, revealing the high affinity of the ACE-2 transmembrane receptors for the SARS-CoV-2 spike protein. Neither the ITO-APTES-mVero nor ITO-APTES-mCalu biosensors showed any significant increase in the electron transfer resistance (c.a. $\Delta R_{ct} = 0.09$ kΩ) after exposure to 25 ng/mL of NS1zikV for 40 min, while a small increase of c. a. $\Delta R_{ct} = 0.36$ kΩ was observed after exposure to 25 ng/mL of NS1denV protein for the same period.

Both cell membrane-based biosensors exhibited a higher affinity for the SARS-CoV-2 spike protein, demonstrating outstanding performance. The EIS response for SARS-CoV-2 spike proteins using the ITO-APTES-

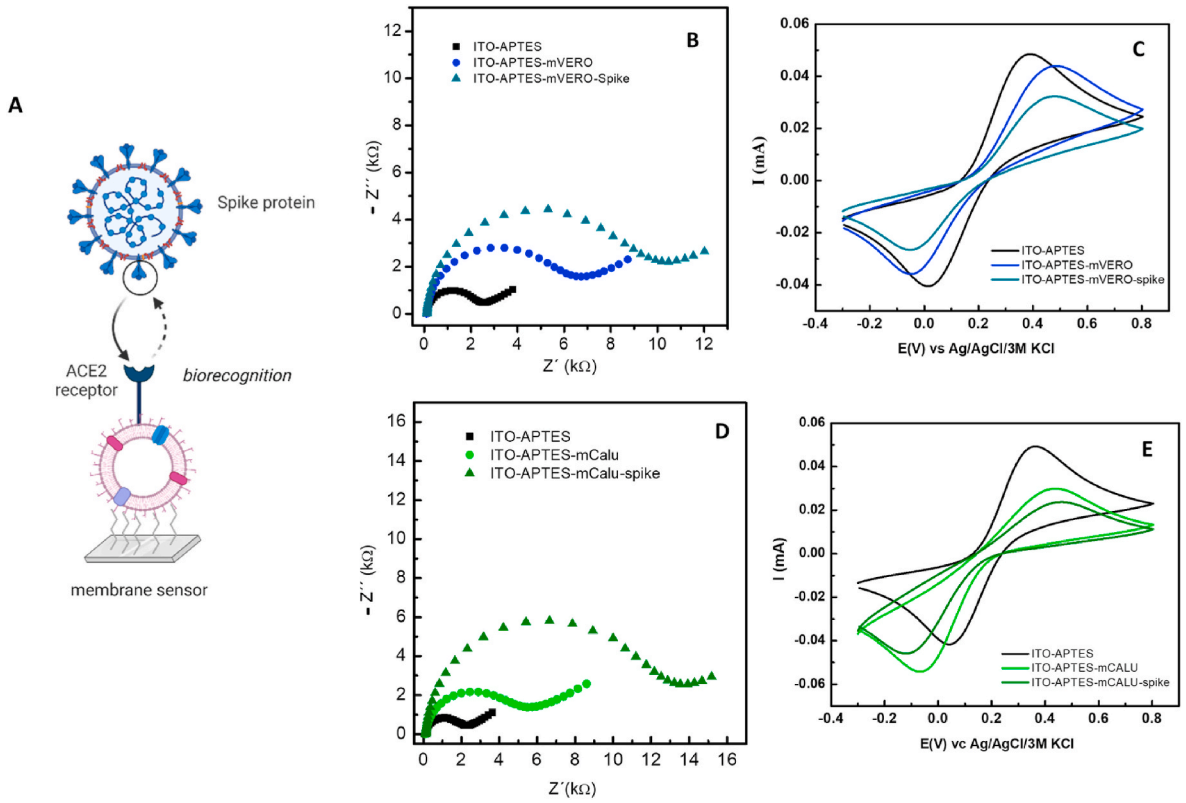

Fig. 3. (A) Schematic representation of the spike protein/membrane biorecognition. Nyquist plots and cyclic voltammograms for ITO-APTES-mVero (B and C) and ITO-APTES-mCalu (D and E). Cyclic voltammograms conditions: $\nu = 100$ mV/s, −300 to 800 mV *vs.* Ag/AgCl/3 M KCl. Nyquist plots conditions: $a = 10$ mV, $f = 10$ kHz to 10 mHz, open circuit. 1.10^7 part/mL mVero and mCalu were immobilized for 1 h and 30 min. Biorecognition with 25 ng/mL of spike protein for 40min. Fig. 3A was created with BioRender.com.

mVero biosensors was 40 and 12 times higher than that observed for NS1zikV and NS1denV proteins, respectively. Similar behavior was noticed for ITO-APTES-mCalu biosensors that showed even higher response signals, with EIS responses 90 and 22 times greater for SARS-CoV-2 spike proteins than for NS1zikV and NS1denV proteins, respectively. This may be associated with the surface modification and arrangement of the ACE-2 receptor binding sites on the electrode surface.

3.4. Analytical parameters

The experimental parameters, including vesicle concentration, incubation time, and SARS-CoV-2 spike protein incubation time, which can affect the detection performance, have been investigated and optimized. As shown in Fig. 4A, a narrow increase in the ΔR_{ct} response was observed when 10^6, 10^7, or 10^8 particles/mL of mVero and mCalu vesicles were immobilized on the electrode surface. In this case, 10^7 particles/mL concentration was chosen for incubation. Three different vesicle incubation times (30, 60, and 90 min) were evaluated and the response of 90 min for both vesicles (Fig. 4B) presented a higher ΔR_{ct} response, which means that more vesicles were bound at the ITO-APTES electrode surface. Finally, the SARS-CoV-2 spike protein incubation times of 10, 20, 40, and 50 min were evaluated. Fig. 4C shows that times below 10 min were sufficient for recognition of the spike protein by the ITO-APTES-mVero biosensor; however, for the ITO-APTES-mCalu biosensors, protein binding times below 20 min were not efficient. However, analysis of the standard deviation at 20 and 40 min indicated the same results, and thus 20 min was chosen as sufficient time for the ACE-2 transmembrane receptors to bind to the SARS-CoV-2 spike protein at the electrodes surface.

To evaluate the relationship between ΔR_{ct} and the spike protein concentration, analytical curves were constructed for each membrane biosensor (ITO-APTES-mVero and ITO-APTES-mCalu) using the previously chosen parameters. Linear regression at the 95% confidence level was used to validate the linearity of the analytical curves. Fig. 4D and E shows the analytical curves for ITO-APTES-mVero and ITO-APTES-mCalu, respectively. It was observed that, as the concentration of the spike protein increased, the ΔR_{ct} values increased, indicating the binding of a higher number of proteins to the immobilized vesicles.

In both cases, a linear increase in ΔR_{ct} was observed upon increasing the SARS-CoV-2 spike protein concentrations. The calibration plot for ITO-APTES-mCalu was linear over the 10–95 ng/mL concentration range ($R^2 = 0.9755$) with the equation: i (nA) = (58 ± 4) [spike] (ng mL ng^{-1}) + (323 ± 241) (nA). The linear range for ITO-APTES-mVero extended between 10 and 110 ng/mL concentration range ($R^2 = 0.9166$) fitting the equation i (nA) = (54 ± 7) [spike] (ng mL ng^{-1}) + (3494 ± 338) (nA). The limit of detection (LOD) and the limit of quantification (LOQ) were estimated according to the $3 \times s_b/m$ and $10 \times s_b/m$ (where s_b is the standard deviation of 10 EIS measurements made in the absence of spike protein and m is the slope of the calibration plot), respectively. The results were LOD = 7.25 pg/mL and LOQ = 21.9 pg/mL for the ITO-APTES-mCalu biosensor, and LOD = 10.0 pg/mL and LOQ = 30.4 pg/mL for the ITO-APTES-mVero biosensor. The R^2 value found for the ITO-APTES-mCalu biosensor (97.55%) indicated a good fit of the system to the linear model. For the ITO-APTES-mVero biosensor, the R^2 (91.66%) was slightly lower than the ITO-APTES-mCalu biosensor value, indicating that the distribution of the points deviates from linearity. The latter may be related to the ACE-2 transmembrane receptor orientation/distribution on the vesicle at the electrode surface.

The repeatability and reproducibility of both membrane biosensors were determined. The relative standard deviation values (%RSD) for repeatability (analysis on the same day) and intermediate precision

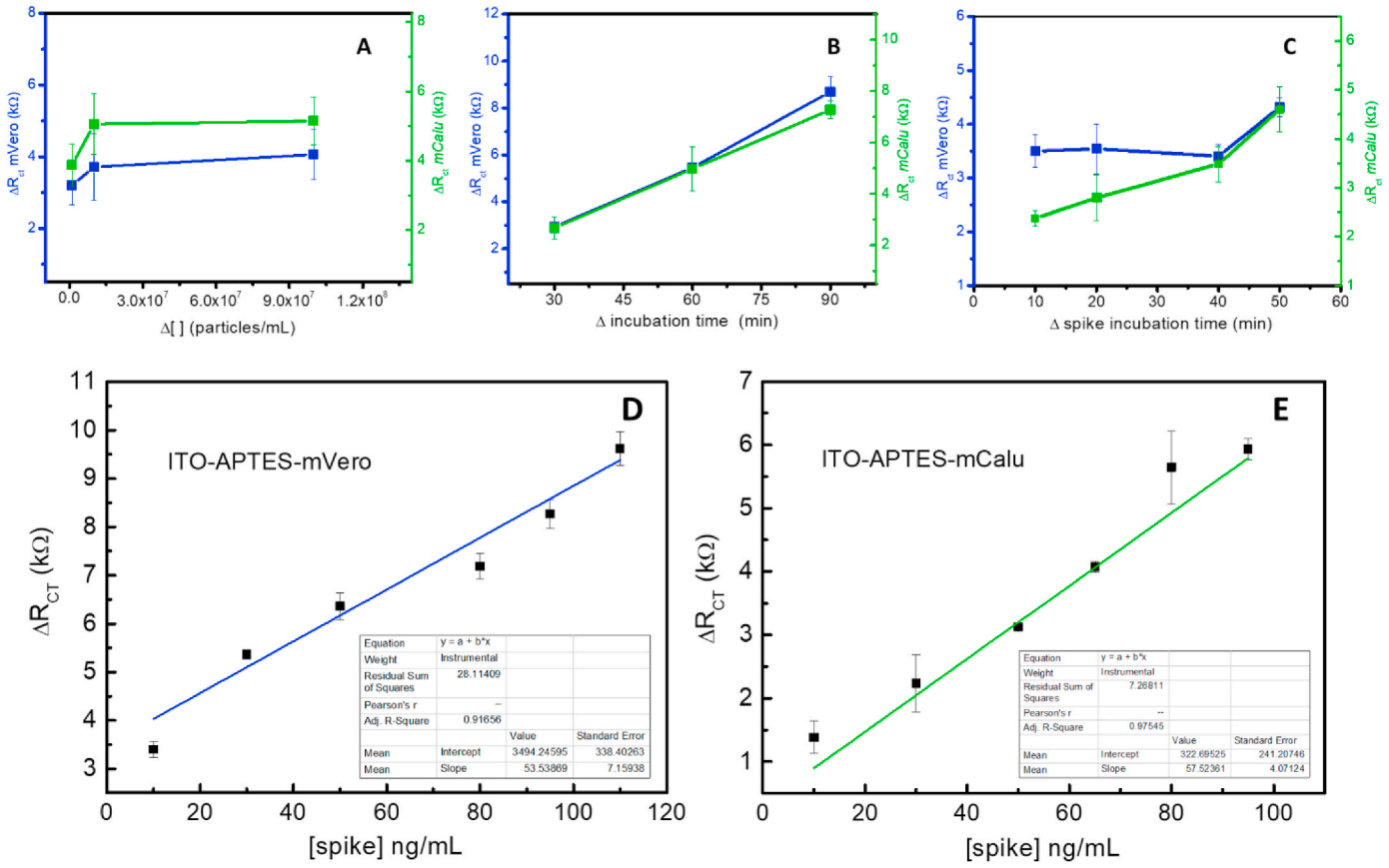

Fig. 4. Analytical features optimization. A) vesicles concentration: (●) mVero ΔR_{ct} values and (●) mCalu ΔR_{ct} values. B) vesicles incubation time: (●) mVero ΔR_{ct} values and (●) mCalu ΔR_{ct} values (at a fixed vesicle concentration of 10^7 particles/mL). C) Different incubation times for the spike protein recognition (●) mVero ΔR_{ct} values and (●) mCalu ΔR_{ct} values (at a fixed concentration of 10^7 particles/mL and time of 20 min). D) Calibration curve from 10 ng/mL to 110 ng/mL to ITO-APTES-mVero and E) Calibration curve from 10 ng/mL to 95 ng/mL to ITO-APTES-mCalu.

(analysis on different days) were estimated using 25 ng/mL of the SARS-CoV-2 spike protein and three electrodes of each analysis. For the ITO-APTES-mCalu biosensor, the %RSD values for repeatability and intermediate precision were 6.07% and 11.0%, respectively, whereas those for the ITO-APTES-mVero biosensor were 5.43% and 23.5%, respectively. The repeatability values of the ITO-APTES-mCalu biosensor were below those required from bioanalytical methods (below 15%), demonstrating the biosensor to be suitable and accurate. The lifetime of the membrane biosensors was evaluated for 20 days, and as shown in Fig. SI-2, both membrane biosensors were stable for this period. It is important to highlight that the lifetime of both membrane biosensors should be evaluated to ensure stability for more long periods, since the vesicle biorecognition layer should be prepared the day before the analysis.

Considering the recently reported electrochemical SARS-CoV-2 sensors applied for spike protein detection, only two of them use the angiotensin-converting enzyme 2 at the electrode surface: RAPIS 1.0, and LEAD [16,17]. These biosensors were able to detect spike proteins via square-wave voltammetry and EIS with good performance. However, those systems differ from that presented here, which uses membranes that express high amounts of ACE-2 transmembrane receptors as immobilized vesicles at the electrode surface, creating a high specificity biorecognition layer. The methodology developed here presents the advantage of simpler construction, wherein protein recognition is performed only by the ACE-2 receptor, without the aid of any nanomaterial or enzymatic labelling. It should also be noted that the total price for the construction of this membrane biosensor was less than a dollar, which is significantly lower than the cost of other sensors that require pure enzymes or antibodies, as described in the literature. This cost considered all materials from cell culture, ultracentrifuge tubes, and chemicals used to construct the membrane biosensors. The use of ACE-2 receptors has also been described as a novel flow cytometry analyses to assess spike-specific antibody responses, with higher specificity, in comparison to commercially available CLIA and ELISA systems [27].

Most systems in the literature consist of antigen/antibody biorecognition or DNA sequences. None of the studies, or patents found, used the entire cell membrane as a biorecognition layer to SARS-CoV-2. The advantage of a receptor-protein system, such as that described herein, is that of obtaining a more specific and low-cost biorecognition layer, since the extraction of these membranes is standardized and uses low-cost laboratory materials, in comparison to obtaining systems such as antigens/antibodies. Although Calu-3 and VeroCCL81 extracted cell membranes contain receptors for pathogens other than SARS-CoV-2, we demonstrated that these membrane biosensors shown satisfactory specificity for the SARS-CoV-2 spike proteins, similar to immunosensors developed with IgG or IgM, as it has been reported in the literature, once this new strategy is based on extracted cell membranes that overexpress ACE-2 receptors as a biorecognition layer. Despite membrane biosensor exhibited some impedimetric response to NS1 proteins, the response for the spike protein was much higher, a property which has not been found in any of the other studies or biosensor patents/sensor devices for SARS-CoV-2. However, even though the developed membrane biosensors exhibit improved qualitative screening (i.e., “yes” or “no” detection) for spike protein recognition, RT-PCR should remain applicable as the gold standard technique for SARS-CoV-2 determination.

4. Conclusion

In this study, biosensors for SARS-CoV-2 detection based on Vero and Calu-3 whole cell membranes were developed. The ITO-APTES-mVero and ITO-APTES-mCalu biosensors were able to detect the SARS-CoV-2 spike proteins in a concentration range from 10 to 100 ng/mL. The limit of detection and the limit of quantification achieved for both systems were 7.25 pg/mL and 21.9 pg/mL for the ITO-APTES-mCalu, and 10.0 pg/mL and 30.4 pg/mL for the ITO-APTES-mVero biosensor, respectively. The EIS studies demonstrated that the biosensors could differentiate between SARS-CoV-2 spike proteins from other biomarker proteins, such as NS1 from the dengue and Zika viruses. This new system may present new opportunities for the development of more efficient, quick, and low-cost diagnoses for SARS-CoV-2, increasing the chances of successful control/isolation of positive patients during the pandemic, and minimising the chances of false positives from other viral diseases.

Credit author statement

Juliana Cancino-Bernardi: Conceptualization, Investigation, Methodology, Formal analysis, Writing – original draft & editing. Edson José Comparetti: Methodology, Formal analysis – vesicles formation and analysis, Writing – review & editing. Natalia Noronha Ferreira: Methodology, Formal analysis – vesicles formation and analysis, Writing – review & editing. Renata Rank Miranda: Methodology, Formal analysis – cell membrane extracted, Writing – review & editing. Marco Montero Tuesta: Methodology, Formal analysis – AFM measurements. Isabella Sampaio: Methodology, Formal analysis – RAMAN measurements and discussion, Writing – review & editing. Paulo Inácio da Costa: Writing – review & editing, Supervision. Valtencir Zucolotto: Conceptualization, Supervision, Writing – review & editing, Funding acquisition.

Declaration of competing interest

The authors declare that they have no known competing financial interests or personal relationships that could have appeared to influence the work reported in this paper.

Data availability

No data was used for the research described in the article.

Acknowledgments

The authors are grateful to FAPESP, CAPES, and CNPq for their financial assistance.

Appendix A. Supplementary data

Supplementary data to this article can be found online at https://doi.org/10.1016/j.talanta.2022.124008.

References

[1] N. Sethuraman, S.S. Jeremiah, A. Ryo, Interpreting diagnostic tests for SARS-CoV-2, JAMA, J. Am. Med. Assoc. 323 (2020) 2249–2251, https://doi.org/10.1001/jama.2020.8259.

[2] T. Chaibun, J. Puenpa, T. Ngamdee, N. Boonapatcharoen, P. Athamanolap, A. P. O'Mullane, S. Vongpunsawad, Y. Poovorawan, S.Y. Lee, B. Lertanantawong, Rapid electrochemical detection of coronavirus SARS-CoV-2, Nat. Commun. 12 (2021) 1–10, https://doi.org/10.1038/s41467-021-21121-7.

[3] R.R. de Assis, A. Jain, R. Nakajima, A. Jasinskas, J. Felgner, J.M. Obiero, P. J. Norris, M. Stone, G. Simmons, A. Bagri, J. Irsch, M. Schreiber, A. Buser, A. Holbro, M. Battegay, P. Hosimer, C. Noesen, O. Adenaiye, S. Tai, F. Hong, D. K. Milton, D.H. Davies, P. Contestable, L.M. Corash, M.P. Busch, P.L. Felgner, S. Khan, Analysis of SARS-CoV-2 antibodies in COVID-19 convalescent blood using a coronavirus antigen microarray, Nat. Commun. 12 (2021), https://doi.org/10.1038/s41467-020-20095-2.

[4] C.M. Das, Y. Guo, D.P. Poenar, Y. Ramaswamy, J. Xiong, M. Yin, K. Yong, In-Depth Conceptual Study of an Enhanced Plasmonic Sensing System Using Antire Fl Ective Coatings and Perovskites for the Detection of Infectious Viral Antigens, 2022.

[5] E. Valera, A. Jankelow, J. Lim, V. Kindratenko, A. Ganguli, K. White, J. Kumar, R. Bashir, Covid-19 point-of-care diagnostics: present and future, ACS Nano 15 (2021) 7899–7906, https://doi.org/10.1021/acsnano.1c02981.

[6] A. Miller, A. Leach, J. Thomas, C. McAndrew, E. Bentley, G. Mattiuzzo, L. John, A. Mirazimi, G. Harris, N. Gamage, S. Carr, H. Ali, R. Van Montfort, T. Rabbitts, A super-potent tetramerized ACE2 protein displays enhanced neutralization of SARS-CoV-2 virus infection, Sci. Rep. 11 (2021) 1–13, https://doi.org/10.1038/s41598-021-89957-z.

[7] M. Letko, A. Marzi, V. Munster, Functional assessment of cell entry and receptor usage for SARS-CoV-2 and other lineage B betacoronaviruses, Nat. Microbiol. 5 (2020) 562–569, https://doi.org/10.1038/s41564-020-0688-y.

[8] M.A.M. Markus Hoffmann, Hannah Kleine-Weber, Simon Schroeder, Nadine Krüger, Tanja Herrler, Sandra Erichsen, Tobias S. Schiergens, Georg herrler, nai-huei Wu, andreas nitsche, S.P. Christian drosten, SARS-CoV-2 cell entry depends on ACE2 and TMPRSS2 and is blocked by a clinically proven protease inhibitor, Cell 181 (2020) 271–280, https://doi.org/10.1016/j.cell.2020.02.052.

[9] S. Lukassen, R.L. Chua, T. Trefzer, N.C. Kahn, M.A. Schneider, T. Muley, H. Winter, M. Meister, C. Veith, A.W. Boots, B.P. Hennig, M. Kreuter, C. Conrad, R. Eils, SARS-CoV-2 receptor ACE2 and TMPRSS2 are primarily expressed in bronchial transient secretory cells, EMBO J. (2020), e105114, https://doi.org/10.15252/embj.2020105114.

[10] M.M. Lamers, J. Beumer, J. Van Der Vaart, K. Knoops, J. Puschhof, T.I. Breugem, R. B.G. Ravelli, J.P. Van Schayck, A.Z. Mykytyn, H.Q. Duimel, E. Van Donselaar, S. Riesebosch, H.J.H. Kuijpers, D. Schipper, W.J.V. De Wetering, M. De Graaf, M. Koopmans, E. Cuppen, P.J. Peters, B.L. Haagmans, H. Clevers, SARS-CoV-2 productively infects human gut enterocytes, Science 369 (2020) 50–54, https://doi.org/10.1126/science.abc1669, 80-.

[11] A. Subramanian, K. Vernon, M. Slyper, J. Waldman, M. Luecken, K. Gosik, D. Dubinsky, M. Cuoco, K. Keller, J. Purnell, L. Nguyen, D. Dionne, O. Rozenblatt-Rosen, A. Weins, A. Regev, A. Greka, RAAS Blockade, Kidney Disease, and Expression of ACE2 , the Entry Receptor for SARS-CoV-2, in Kidney Epithelial and Endothelial Cells, 2020, pp. 1–28, https://doi.org/10.1101/2020.06.23.167098.

[12] L. Chen, X. Li, M. Chen, Y. Feng, C. Xiong, The ACE2 expression in human heart indicates new potential mechanism of heart injury among patients infected with SARS-CoV-2, Cardiovasc. Res. 116 (2020) 1097–1100, https://doi.org/10.1093/CVR/CVAA078.

[13] X. Zou, K. Chen, J. Zou, P. Han, J. Hao, Z. Han, Single-cell RNA-seq data analysis on the receptor ACE2 expression reveals the potential risk of different human organs vulnerable to 2019-nCoV infection, Front. Med. 14 (2020) 185–192, https://doi.org/10.1007/s11684-020-0754-0.

[14] N.M. Id, A.G. Therien, B.H. Id, D. Klein, K.K. Id, L.A. Lieberman, G.C.A. Id, J.F. Id, P. Mckenna, G. Swaminathan, D.J. Hazuda, D.B.O. Id, Propagation : Considerations for Drug Discovery and Development, 2021, pp. 1–18, https://doi.org/10.1371/journal.ppat.1009225.

[15] K. Takayama, Trends in pharmacological sciences in vitro and animal models for SARS-CoV-2 trends in pharmacological sciences, Trends Pharmacol. Sci. xx (2020) 1–4, https://doi.org/10.1016/j.tips.2020.05.005.

[16] M.D.T. Torres, W.R. de; Araujo, L.F. de; Lima, A.L. Ferreira, C. de la Fuente-Nunez, Low-cost biosensor for rapid detection of SARS-CoV-2 at the point of care, Matter 4 (2021) 2403–2416, https://doi.org/10.1016/j.matt.2021.05.003.

[17] L.F. De Lima, A.L. Ferreira, M.D.T. Torres, W.R. De Araujo, Minute-scale detection of SARS-CoV-2 using a low-cost biosensor composed of pencil graphite electrodes, Proc. Natl. Acad. Sci. USA 118 (2021) 1–9, https://doi.org/10.1073/pnas.2106724118/-/DCSupplemental.Published.

[18] R. Lund, R. Leth-Larsen, O.N. Jensen, H.J. Ditzel, Efficient isolation and quantitative proteomic analysis of cancer cell plasma membrane proteins for identification of metastasis-associated cell surface markers, J. Proteome Res. 8 (2009) 3078–3090, https://doi.org/10.1021/pr801091k.

[19] ICH, Guidance for industry, Q2B validation of analytical procedures: methodology, Int. Conf. Harmon. Tech. Requir. Regist. Tripart. Guidel. 13 (1996) https://doi.org/62 FR 27464.

[20] E.M. Agency, European Medicines Agency: an Unacceptable Choice, Prescrire Int., 2011, p. 278.

[21] V.S. Marangoni, J. Cancino Bernardi, I.B. Reis, W.J. Fávaro, V. Zucolotto, Photothermia and activated drug release of natural cell membrane coated plasmonic gold nanorods and β-lapachone, ACS Appl. Bio Mater. 2 (2019), https://doi.org/10.1021/acsabm.8b00603.

[22] E.J. Comparetti, P.M.P. Lins, J.V.B. Quitiba, V. Zucolotto, Cancer cell membrane-derived nanoparticles improve the activity of gemcitabine and paclitaxel on pancreatic cancer cells and coordinate immunoregulatory properties on professional antigen-presenting cells, Mater, Adv (2020), https://doi.org/10.1039/D0MA00367K.

[23] J. Cancino-Bernardi, P.M.P. Lins, V.S. Marangoni, H.A.M. Faria, V. Zucolotto, Difference in lipid cell composition and shaped-based gold nanoparticles induce distinguish pathways in Langmuir monolayers response, Mater. Today Commun. 26 (2021), https://doi.org/10.1016/j.mtcomm.2020.101831.

[24] R. Chandrasekhar, K.L. Choy, Innovative and cost-effective synthesis of indium tin oxide films, Thin Solid Films 398 (2001) 59–64, https://doi.org/10.1016/S0040-6090(01)01434-1.

[25] J. Surmacki, B. Brozek-Pluska, R. Kordek, H. Abramczyk, The lipid-reactive oxygen species phenotype of breast cancer. Raman spectroscopy and mapping, PCA and PLSDA for invasive ductal carcinoma and invasive lobular carcinoma. Molecular

tumorigenic mechanisms beyond Warburg effect, Analyst 140 (2015) 2121–2133, https://doi.org/10.1039/c4an01876a.

[26] D. Bhowmik, K.R. Mote, C.M. MacLaughlin, N. Biswas, B. Chandra, J.K. Basu, G. C. Walker, P.K. Madhu, S. Maiti, Cell-membrane-mimicking lipid-coated nanoparticles confer Raman enhancement to membrane proteins and reveal membrane-attached amyloid-β conformation, ACS Nano 9 (2015) 9070–9077, https://doi.org/10.1021/acsnano.5b03175.

[27] D. Lapuente, C. Maier, P. Irrgang, J. Hübner, A.S. Peter, M. Hoffmann, A. Ensser, K. Ziegler, T.H. Winkler, T. Birkholz, A.E. Kremer, P. Steininger, K. Korn, F. Neipel, K. Überla, M. Tenbusch, Rapid response flow cytometric assay for the detection of antibody responses to SARS-CoV-2, Eur. J. Clin. Microbiol. Infect. Dis. (2020) 751–759, https://doi.org/10.1007/s10096-020-04072-7.